Journal of Materials Chemistry A

Accepted Manuscript

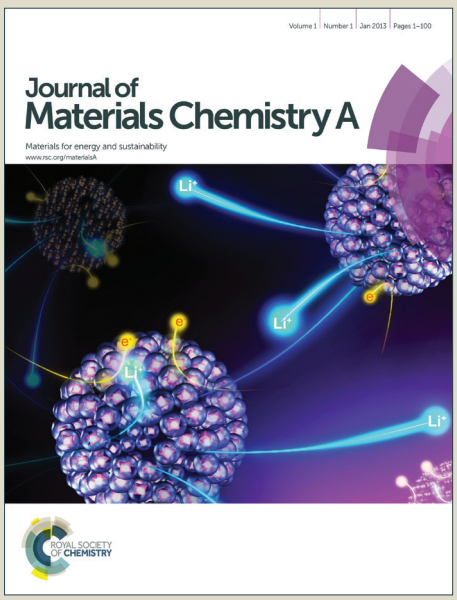

ROYAL SOCIETY OF CHEMISTRY

www.rsc.org/materialsA

Journal Name

ARTICLE

A catalyst superior to carbon-supported-platinum for promotion of the oxygen reduction reaction: reduced-polyoxometalate supported palladium

Received 00th January 20xx,
Accepted 00th January 20xx

DOI: 10.1039/x0xx00000x

www.rsc.org/

Xiaohong Xie, Yao Nie, Siguo Chen, Wei Ding, Xueqiang Qi, Li Li and Zidong Wei*

The high solubility of Polyoxometalates (POMs) in basic electrolyte limits their practical applications. Fortunately, we found this shortcoming can be overcome by electrochemically reducing the POMs. The reduced POMs (rPOM) are extremely stable in alkaline solution and can participate in electrocatalytic cycles. Herein, we present novel rPOM as a Pd-catalyst-substrate to achieve a high catalytic performance towards the oxygen reduction reaction (ORR). Interestingly, although rPOM alone has very low catalytic activity, the Pd/rPOM hybrid catalyst exhibits excellent electrocatalytic performance for ORR in alkaline media, even better than the commercial Pt/C catalyst. The much improved ORR activity of Pd/rPOM is based on electron delocalization between the Pd and the rPOM support, causing a down-shift in the d-band structure of the Pd NPs. Furthermore, the rPOM in the Pd-rPOM hybrid serves as an assistant catalyst, facilitating the decomposition of the harmful hydrogen peroxide intermediates. The method reported here will promote broader interest in the further development of other new catalysts for real-world applications.

Introduction

The oxygen reduction reaction (ORR) is one of the most crucial factors limiting the performance of fuel cells due to its sluggish kinetics. Thus, the development of efficient ORR electrocatalysts is of great significance. With respect to the mainstream catalysts for ORR, today's platinum-based catalysts severely suffer from high cost and poor durability, which hampers large-scale application of fuel cells.[1] Therefore, economical and effective alternative catalysts are highly required. Among the metal-based catalysts studied to date, palladium (Pd), which is considerably less expensive than Pt, has been widely investigated because of its functional similarities to Pt.[2] Although many recent strategies have focused on the design of new catalyst structures,[3] alloying of Pd with other metals,[4] modification of Pd with other species,[5] and optimization of the catalysts structure to increase the exposure of Pd nanoparticles (NPs) to the three-phase zone,[6] the activities and stabilities of these Pd-based catalysts are still barely equivalent to typical Pt containing materials. The development of high performance Pd-based catalysts for ORR remains a great challenge.

Recently, the synergetic effect on heterogeneous composite catalysts has attracted great attention because the combination of catalytic component and support materials can sometimes endow the composite catalysts with unexpectedly improved catalytic properties.[7] For example, highly-durable oxide substrates are introduced to promote the reactivity of metal-based catalysts *via* strong electron coupling between metal and substrates, as well as the compositional and structural complexity of such supported catalysts systems offers many degrees of freedom for tuning their catalytic activity.[8] However, the innate low conductivity of oxide materials prevents their use in an electrochemical device, where electrons are either reactants or products; therefore, good electrical conductance is absolutely required. On the other hand, for most of currently support materials, they have no access for proton, which is of vital importance because the performance of electrode materials for fuel cells are also relevant to proton-transfer and structural re-organization, which are both required for fast proton conductivity.[9] Materials conducting both electron and proton are urgently desired to make catalyst achieve full utilization. In this background, catalysts coupled with polyoxometalates (POMs) have been identified.[10] POMs, which are nanoscale transition metal-oxygen clusters, have been exploited in a wide range of electrochemical applications due to their multiple properties such as efficient electron pathways, high proton conductive, excellent water tolerance and high catalytic active.[11] Nevertheless, the use of POMs for the promotion of electrocatalytic reactions is still in its infancy. Only a few illustrations including POMs-loaded composites to different mesoporous hosts as support for metal NPs have been reported, all focusing on the immobilization of POMs.[12] More specifically, the high solubility of POMs in basic electrolyte is still one of the most critical problems that must be solved in order to find their practical applications in an electrochemical system.

Fortunately, we found that this shortcoming can be overcome by electrochemically reducing the POMs. The reduced POMs,

Chongqing Key Laboratory of Chemical Process for Clean Energy and Resource Utilization, School of Chemistry and Chemical Engineering, Chongqing University, Chongqing 400044, PR China
Email: zdwei@cqu.edu.cn
Electronic Supplementary Information (ESI) available: [BET and XPS patterns, TEM images, and CVs]. See DOI: 10.1039/x0xx00000x

or the so-called heteropoly blue, are extremely stable in alkaline solutions (as detailed in Fig. S1). They can accept or release a specific numbers of electrons without change or decomposing in their structural arrangements. Furthermore, redox systems based on POMs are electrochemically fast, thus the reduced POMs can participate in numerous electrocatalytic cycles. Based on the above considerations, it is possible to use reduced POMs as a catalyst or assistant catalyst substrate in oxidation-reduction reactions. In this study, we present a novel strategy to address the solubility issue of POM *via* forming a reduced layer onto its surface (rPOM), and the resulting rPOM particles with high stability were employed as an ameliorative Pd NPs support to achieve a high catalytic performance. We demonstrate that the serious corrosion of POM can be alleviated due to the protection of the reduced-POM outer cover. The use of rPOM as a support for Pd NPs not only enhances the stability of the Pd NPs *via* powerful support interactions but also efficiently enhances the ORR activity of the Pd NPs *via* electron transfer between Pd and rPOM.

Experimental Section

Preparation of POM ($(NH_4)PMo_{12}O_{40}$): POM was synthesised by a simple method.[13] In brief, 0.01 mol $(NH_4)_2MoO_4$ and 0.012 mol H_3PO_4 were first dissolved in 200 mL of pure water. Then, 10 mL of a concentrated HNO_3 solution was poured, drop by drop, into the above solution to precipitate the yellow-coloured POM. The POM was filtered, washed with 1 wt% HNO_3 solution and dried at room temperature over several days.

***The synthesis of Pd/rPOM and Pd/C catalysts*:** Pd/rPOM and Pd/C were synthesised *via* the $NaBH_4$ reduction method. The loading of Pd was deliberately controlled to be 5 wt % for Pd/rPOM and 20 wt % for Pd/C in consideration of the difference in the specific surface area (Fig. S2) between POM and C. Briefly, a deaerated suspension of the POM support (or activated carbon) and trisodium citrate dehydrate (TCD), a solution of $NaBH_4$, and a Pd precursor ($PdCl_2$) dissolved in an aqueous HCl solution were prepared separately. The three solutions were mixed together and then stirred for 2 h to allow the adsorption of the colloidal Pd particles onto the support. It is interesting to note that the POM was reduced (*in-situ*) at the same time as Pd precursor was reduced to form the Pd/rPOM hybrid (see Fig. 1). The product was subsequently filtered, washed, and vacuum dried at 80 °C. For comparison, a separate rPOM was also prepared following the same method as used in the preparation of the Pd/rPOM catalyst, only without the Pd precursor.

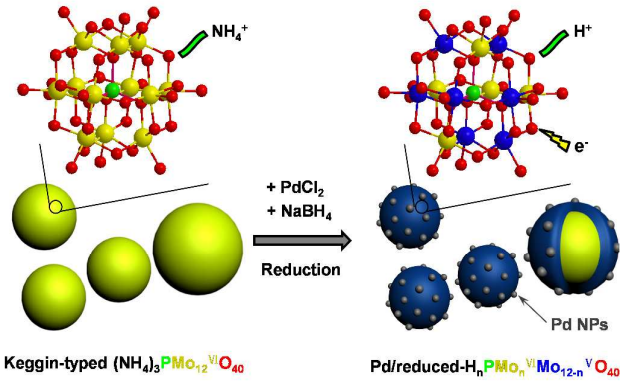

Fig. 1 Schematic illustration for the fabrication of the Pd/rPOM hybrid catalyst.

The Pd content in the Pd-based catalysts was determined by spectrophotometric determination. Briefly, the Pd catalyst was calcined at 900 °C for 1 h to remove the rPOM (or carbon) and was then dissolved in nitrohydrochloric acid. After the solvent was evaporated, the dissolved solid remained in HCl solution. The Pd-containing solution was placed in a 100 mL brown volumetric flask, and 2 mL of HCl (1:1), 3 mL of an EDTA solution, 4 mL of a sodium sulfite solution, and 2.5 mL of a potassium iodide solution were added. The solution was diluted with water to the mark and kept in the dark for 15 min before the absorbance was measured at 490 nm. The Pd mass contents of Pd/rPOM and Pd/C materials were determined to be 4.19 wt % and 19.66 wt %, respectively. The estimated Pd loading on the rPOM support is nominally agreed with the EDAX results.

***Material characterization*:** A Micromeritics ASAP 2020 accelerated surface area and porosimetry analyzer was used to determine the BET surface specific area of carbon and POM support. X-ray diffraction data were collected on a XRD-6000 using Cu KR radiation (λ=1.5418 Å) at a step rate of $2°\cdot min^{-1}$. Scanning electron microscopy (SEM) was carried out on a LEO-1530VP instrument. Both low-resolution transmission electron microscopy (TEM) and high-resolution transmission electron microscopy (HRTEM) were conducted on a FEI tecnai G^2 20S-TWIN instrument operating at 120 kV. X-ray photoelectron spectroscopy was conducted on a Cratos XSAM800 spectrometer equipped with a monochromatic Al X-ray source (Al KR, 1.4866 keV). The vacuum in the analysis chamber was maintained at 10^{-7} Pa, and the binding energy was calibrated using 285 eV as the C 1s peak energy.

Electrochemical measurements: All experiments for the synthesized electrocatalysts were performed using Princeton electrochemical workstation in a standard three-electrode cell. The catalyst particles were deposited on a glassy carbon (GC) disk electrode (Pine Instruments, Grove City, PA). A leak-free AgCl/Ag/KCl (3M) electrode (Warner Instrument) was used as the reference. All potentials have been converted to the values with reference to the RHE. The electrolyte was 0.1 M KOH solution. A platinum wire was used as counter electrode. A glassy carbon (GC) disk electrode with a diameter of 5 mm and a geometric area of 0.1963 cm^2 was polished with 0.05 μm alumina before each experiment and used as a working electrode. For the electrode preparation, the catalyst was dispersed in ethanol and sonicated for 15 minutes to form a uniform catalyst ink, and 20 μL of this ink was pipetted onto the GC disk. After the solvent was evaporated, the deposited catalyst was covered with a drop of dilute aqueous Nafion solution (0.1 wt %). The resulting thin film was strong enough to attach the catalyst particles permanently to the GC RDE without producing any resistance. The prepared electrodes were dried at room temperature for 20 minutes before electrochemical testing. All electrochemical measurements were conducted 3 times to avoid any incidental error.

The specific kinetic current (i_k) associated with the intrinsic activity of the catalysts can be obtained based on the following equation:

$$i_k = \frac{i_d i}{i_d - i}$$

where i is the experimentally obtained current, i_d refers to the measured diffusion-limited current (in the potential region below 0.5 V), and i_k is the mass-transport free kinetic current. The numbers of electrons transferred (n) during the course of the ORR were calculated for Pd/rPOM, and the Pd/C and Pt/C catalysts, from the RDE voltammetric results obtained at electrode rotation speeds using the Koutecky-Levich (K-L) equation:

$$i_d = 0.62nFACD^{2/3}\nu^{-1/6}\omega^{1/2}$$

where n is the number of electrons transferred, F is the Faraday's constant (96485 C·mol^{-1}), A is the area of the electrode (0.19625 cm^2), C is the saturated concentration of oxygen (1.2×10^{-3} mol·L^{-1}), D is the diffusion coefficient of oxygen in 0.1 M KOH solution (1.9×10^{-5} cm^2·s^{-1}), ν is the kinematic viscosity of the solution (0.01 cm^2·s^{-1}), and $\omega = 2\pi f/60$, f is the RDE rotation rate in rpm. Mass activities and specific activities were determined *via* calculation of i_k and normalized with the noble metal (Pd or Pt) loading and the electrochemically active surface area (ECSA), respectively.

All Rotating Ring-Disk Electrode (RRDE) measurements were conducted using 0.1 M KOH. A glassy carbon (GC) ring-disk electrode with a ring geometric area of 0.1866 cm^2 (diameter 5.61 mm) and a disk geometric area of 0.2475 cm^2 was used as working electrode. In the RRDE experiments, the ring potential was set to 1.1 V vs. RHE. Before the experiments, the Pt catalyst in the ring was activated through potential cycling in the electrolyte from 0 to 1.2 V at a scan rate of 50 mV·s^{-1} for 50 cycles. The four-electron selectivity of catalysts was evaluated based on the H_2O_2 yield, which was calculated from the following equation:

$$H_2O_2\% = 200\frac{i_{ring}/N}{i_{disk}+i_{ring}/N}$$

where i_{disk} and i_{ring} are the disk and ring currents, respectively, and N is the ring collection efficiency (37%).

Results and Discussion

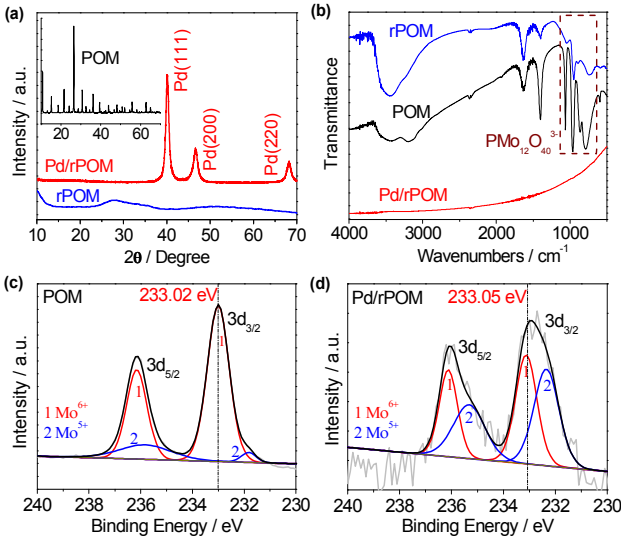

Fig. 2 (a) XRD patterns and (b) FT-IR spectra of all the samples; (c) Mo 3d of POM and (d) Mo 3d of Pd/POM.

The phase and purity of the as-prepared Pd/rPOM powders were determined by XRD. In Fig. 2a, well-resolved diffraction peaks at 2θ values of 40.1°, 46.6° and 68.1° are indexed as the Pd(111), Pd(200) and Pd(220) planes, indicating a face-centered cubic crystal structure for the Pd grown on the rPOM. However, diffraction peaks corresponding to crystalline POM phase (insert in Fig. 2a) are not observed in the Pd/rPOM powders because the inner POM is covered by a thick rPOM layer, which only exhibits a weak XRD diffraction relative to the crystalline Pd NPs. With a strong reduction process, the outside surface of POM should be reduced totally together with Pd ions reduction to form a reduced Pd/rPOM; the Pd NPs are set on the rPOM rather than on the POM as illustrated in Fig. 1 even though the inner POM may not be fully reduced. Furthermore, the reduction of POM is accompanied by both electronization and protonation.[14] In order to gain further insight into the structures of all the samples, Fourier transform IR spectroscopy (FT-IR) spectra of POM, rPOM and Pd/rPOM hybrid were measured as shown in Fig. 2b. The spectra of POM and rPOM show peaks located at approximately 785 (ν_{as}(Mo-O), edge sharing bonds), 869 (ν_{as}(Mo-O), corner sharing bonds), 962 (ν_{as}(Mo=O)) and 1068 (ν_{as}(P-O)) cm^{-1} that can be assigned to the special keggin-type $[PMo_{12}O_{40}]^{3-}$.[15] This result proves that although the electrochemical reduction of POM causes a change in valence-state, it does not induces structural changes in the anionic cluster. Additionally, it can be seen that Mo-O stretching bands for the rPOM are all red shifted slightly relative to the Mo-O stretching bands observed for the POM, this indicates that strong hydrogen bonds are formed on the oxygen atoms of rPOM. However, the spectrum of the Pd/rPOM powder differs from those of POM and rPOM, showing decreases in band intensity ascribed to absorption of IR radiation by the nano-sized Pd black. Similar results have been reported in polymers in combination with carbon-black-supported Pd catalysts.[16] Overall, the FT-IR spectra provide evidence for the successful preparation of Pd NPs supported on the *in-situ* developed rPOM.

X-ray photoelectron spectroscopy (XPS) carried out on the pristine POM (Fig. S3a) clearly indicated the presence of P and Mo. As shown in Fig. 2c, the Mo doublet with binding energies of 236.17 and 233.02 eV could be assigned to the Mo^{6+} species of pristine POM. The ratio of Mo^{6+} to Mo^{5+} is 85.35/14.65. Whereas in the case of Pd/rPOM (Fig. S3b), the ratio of Mo^{6+} to Mo^{5+} is 48.67/51.33 (Fig. 2d), indicating the partial-reduction of POM to rPOM. Additional XPS peaks shown in Fig. S3b located at approximately 338 eV are attributable to the 3d binding energies of Pd.

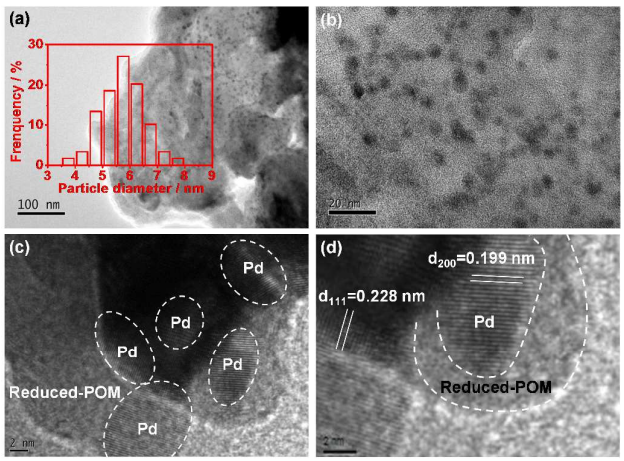

Fig.3 (a)-(b) SEM images of the Pd/rPOM hybrid, insert (a) is the size distribution histogram for the Pd particles; (c)-(d) High-resolution TEM images of Pd NPs supported on the rPOM.

Fig. 3a and 3b show typical scanning electron microscopy (SEM) images of Pd/rPOM. The small, uniformly distributed, darkly contrasting Pd NPs (~5 nm) are clearly well adhered to the support. Magnified transmission electron microscopy (TEM) images (Fig. 3c, d) confirm that the supported Pd NPs are highly crystalline, with the fringe distances of 2.28 Å and 1.19 Å (Fig. 3d) corresponding to the inter-planar spacing of the (111) and (200) planes in the cubic Pd lattice. Energy-dispersive X-ray analysis (EDAX) applied directly to the Pd/rPOM material showed the presence of 4.10 wt % Pd on the rPOM support (Fig. S4). The Pd loading was also confirmed by

spectrophotometric determination, with a qualitative value of 4.19 wt % obtained for the amount of Pd with reference to the rPOM.

The catalytic properties of Pd/rPOM in the ORR were studied alongside home-made Pd/C (20%, as shown in Fig. S4) and commercial Pt/C catalysts for comparison. Fig. 4a shows cyclic voltammograms (CVs) of rPOM and Pd/rPOM recorded in an N_2-saturated 0.1 M KOH electrolyte, respectively. The CVs show a very small current density on the rPOM but very large current density on the Pd/rPOM, indicating the formation of a much larger electrode/electrolyte interfacial area in the Pd/rPOM than obtained on the Pd/C and Pt/C electrodes (Fig. S5). Furthermore, It shows that the Pd/rPOM catalyst has a pair of redox peaks at around 0.7 V, which can be attributed to the electron-involved reversible reduction/oxidation of the rPOM, but mainly can be attributed to the formation of a special Pd-O structure between the Pd and the oxygen-rich anionic clusters of the rPOM that exhibit an overlapped redox peaks. On the other hand, no typical peaks associated with the Pd especially in the area of the hydrogen adsorption/desorption are observed; this may arise from its own support. The large cathodic current of rPOM support seems transferred to the CV profile of its supported Pd catalyst and may be rational to contribute the large cathode current to enhanced hydrogen underpotential deposition current. It should be noted that while the Pt or Pd loadings on all electrodes were the same (~10 ug), but the apparent current density on the Pd/rPOM catalyst is largest. We believe that the greatly increased CV current obtained with the Pd/rPOM catalyst is a result of the so-called spillover effect, where adsorbed OH^- or O^- containing species are spilled over to and back-spilled over from the rPOM, enabled by the strong metal oxide-support interactions between Pd and the protonated rPOM support, as once observed in Pt-based catalysts.[17]

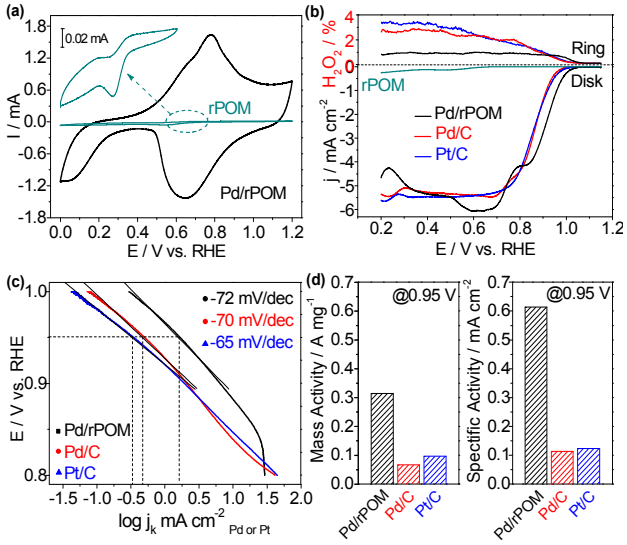

Fig. 4 (a) CVs of Pd/rPOM and rPOM (insert) recorded in a 0.1 M KOH electrolyte (scan rate: 50 mV·s^{-1}); (b) ORR polarization plots (bottom) and the H_2O_2 yield plots (top) measured on the Pd/rPOM, Pd/C and Pt/C-coated RRDE in O_2-saturated 0.1 M KOH electrolyte at room temperature with an RRDE rotation rate of 1600 rpm, a voltage sweep rate of 10 mV·s^{-1} and a ring potential fixed at 1.1 V; (c) Tafel plots from the different catalysts; (d) Mass activities and specific activities for Pd/rPOM, Pd/C and Pt/C at 0.95 V.

ORR measurements performed in an O_2-saturated 0.1 M KOH electrolyte using a glassy carbon rotating ring-disk electrode (RRDE) and catalyzed by different catalysts are shown in Fig. 4b (bottom). After subtraction of the background current recorded in an N_2-saturated 0.1 M KOH electrolyte (Fig. S6), the onset potential of the Pd/rPOM catalyzed ORR is 1.078 V, which is approximately 57 mV and 51 mV more positive than with the Pd/C and Pt/C catalyzed RDE, respectively. At the same time, the Pd/rPOM catalyzed ORR on the RDE has a more positive half-wave potential than either the Pd/C (~49 mV) or Pt/C RDE (~55 mV), confirming that the Pd/rPOM powder is an excellent catalyst for the alkaline ORR. The ring current densities collected on the RRDE, indicating the yield of H_2O_2 intermediates in the ORR on the RDE, reveal the lowest H_2O_2 yield from the Pd/rPOM materials (Fig. 4b, top). This means that O_2 is most likely reduced to water *via* a 4$^-$ electron transfer on the Pd/rPOM electrode. The electron transfer numbers based on Fig. S6 are 3.95, 3.80 and 3.80 on the electrodes containing Pd/rPOM, Pd/C and Pt/C, respectively, in 0.1 M KOH electrolyte. This once again proves the excellent ORR activity of the Pd/rPOM hybrid catalyst.

Fig. 4c presents the mass-corrected Tafel plots of the logarithm of kinetic current density, log J_k (mA·cm^{-2}), *vs.* the electrode potential E for the ORR on the Pd/rPOM, Pd/C and Pt/C electrodes. The Tafel slope of Pd/rPOM (-72 mV·dec^{-1}) over the majority of the high potential range is very close to the values of the Pd/C (-70 mV·dec^{-1}) and Pt/C (65 mV·dec^{-1}) catalysts, suggesting almost the same reaction mechanism of ORR on the different electrodes. Detailed comparisons of the ORR activities of all electrodes normalized against noble metals present in the catalyst were also summarized. As shown in Fig. 4d, the mass activity of the Pd/rPOM catalyst was measured to be 0.315 A·mg^{-1}, which is much higher than those of Pd/C (0.0672 A·mg^{-1}) and Pt/C (0.0969 A·mg^{-1}) catalysts. Similarly, specific activities of all the samples were obtained from mass-transport-corrected Tafel plots by normalizing the kinetic current to the electrochemically active surface area (ECSA). Generally, the ECSA of Pt-based catalysts are measured with underpotential deposition and stripping of hydrogen. It is assumed that each surface platinum atom is associated with one chemisorbed hydrogen atom, allowing the charge corresponding to the area under the hydrogen adsorption peaks to be converted to the real ECSA. However, for Pd-based catalysts, the method based on the hydrogen adsorption charge seems to be less reliable because Pd can absorb large quantities of hydrogen (up to 900 times its own volume). The real ECSA of Pd-based catalysts are determined by considering the Columbic charges corresponding to the monolayer PdO reduction.[18] Herein, it is not possible to measure the ECSA value of Pd/rPOM catalyst accurately by using this method because no typical peaks associated with the PdO reduction was observed under the measurement condition (0.1 M KOH solution). The very large O-species reduction peaks may influenced by the spillover-effect between Pd and the rPOM support. Fortunately, we found that this effect can be substantially alleviated under an acidic condition. Therefore, the ECSA of catalysts in this work can be approximately obtained using the methods described above whereas under the measurement condition of 0.1 M $HClO_4$. As shown in Fig. 5, the ECSA for Pd-based catalyst was calculated by measuring the charge associated with the PdO reduction region after double-layer correction from the CVs, assuming a value to 0.405 mC·cm^{-1} for the monolayer PdO reduction into Pd on the Pd surface, while the ECSA for Pt-based catalyst was obtained by assuming that the monolayer hydrogen desorption charge is

0.210 mC·cm^{-1} on the Pt surface for Pt-based catalyst. The ECSA of the Pd/rPOM, Pd/C and Pt/C is about 51.17, 46.33 and 78.62 m^2·g^{-1}, respectively: this is in good accord with their corresponding Pd or Pt particle size as revealed by TEM. The specific activity of three catalysts, Pd/rPOM, Pd/C and Pt/C at 0.95 V based on their ECSA is 0.615, 0.114 and 0.123 mA·cm^{-2}, respectively, as shown in Fig. 4d. It indicates that the Pd/rPOM hybrid developed in this work is more active for the ORR than Pd/C and even Pt/C catalyst in alkaline media.

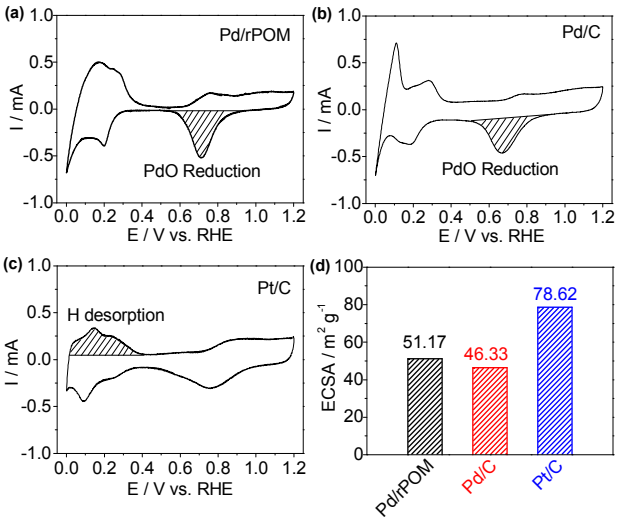

Fig. 5 CV curves for (a) Pd/rPOM, (b) Pd/C, and (c) Pt/C catalysts. Data was collected at 50 mV·s^{-1} in an N_2-saturated 0.1 M $HClO_4$ electrolyte. (d) Normalized ECSAs of all catalysts.

To gain understanding of the durability of the catalysts under potential cycling conditions, we subjected the catalysts to 1500 cycles between 0 and 1.2 V in a N_2-saturated 0.1 M KOH electrolyte (Fig. 6). After 1500 potential cycles, the CV profile for Pd/rPOM changes little (Fig. 6a), while large change were observed for the Pd/C (Fig. 6c) and Pt/C (Fig. 6e) catalysts, indicating a far greater stability for the Pd/rPOM catalyst than for the Pd/C and Pt/C materials. The ORR performance of the catalyst, as measured by liner potential sweeping in O_2-saturated 0.1 M KOH before and after 1500 potential cycles, showed no noticeable degradation of the Pd/rPOM catalyst electrode (Fig. 6b), but a 41 mV (Fig. 6d) and 45 mV (Fig. 6f) decline in the half-wave potential for the Pd/C and Pt/C catalyzed electrodes, respectively. Simultaneously, the diffusion-limiting current decreased significantly for the Pd/C and Pt/C catalyzed electrode, indicating the loss of Pd or Pt NPs from the electrode. Calculation of the mass activity (@0.95 V) for Pd/rPOM showed no recordable loss of Pd activity. In a sharp contrast, a serious loss of activity was observed corresponding Pd/C and Pt/C catalysts. The activity of Pd/C showed a degradation of 86.49%, while Pt/C reduced by 90.83%, suggesting that carbon corrosion at high potentials was responsible for this effect; in other words, rPOM is stable enough to endure the harsh corrosive environment.

The Pd 3d XPS spectra of the Pd/C and Pd/rPOM catalysts before and after durability cycling also provided compelling evidence of the excellent stability of the Pd/rPOM catalyst in comparison with Pd/C. The Pd/rPOM catalyst (Fig. 7a) exhibited no change in the Pd 3d XPS spectra after durability cycling, in agreement with the maintenance of the ORR activity after durability testing (Fig. 6b). Unfortunately, a positive shift (~0.69 eV) in the Pd 3d binding energy in the Pd/C catalyst was observed after durability cycling (Fig. 7b). This positive shift in binding energy can be ascribed to particle aggregation due to the poor interaction between the Pd NPs and the C support. These results indicate that the Pd/rPOM catalyst is both chemically and electrochemically more stable than the Pd/C catalyst.

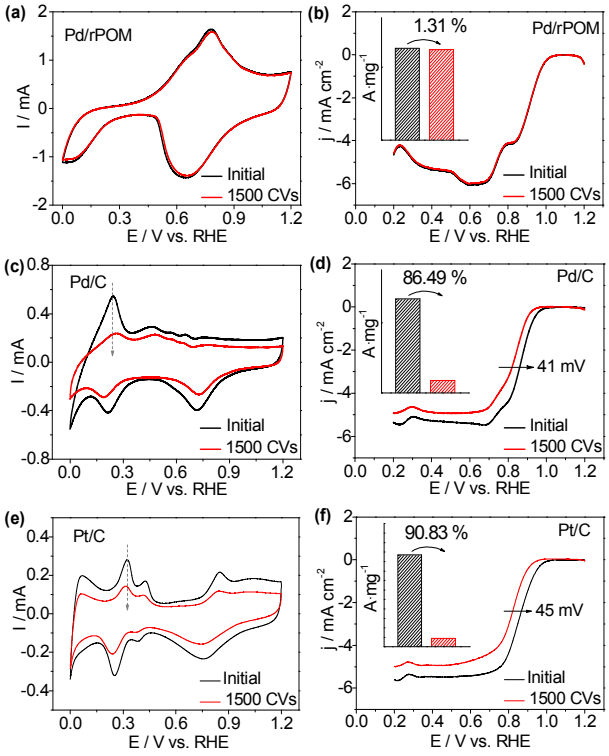

Fig. 6 CV curves for (a) Pd/rPOM, (c) Pd/C and (e) Pt/C before and after the stability tests in O_2 saturated 0.1 M KOH; ORR curves for (b) Pd/POM, (d) Pd/C and (f) Pt/C before and after the stability tests in O_2 saturated 0.1 M KOH; scan rate: 10 mV·s^{-1}; rotating rate, 1600 rpm.

Both activity and durability studies indicate that rPOM could serves as an efficient support material, enhancing the performance of Pd NPs toward ORR. These enhancements represent an interesting phenomenon worthy of further investigation. Generally, O_2 activation involves both proton and electron transfer to form adsorbed oxygen-containing intermediate species (O_{ads}, e.g., H_2O_2) before the O-O bond is broken.[19] Therefore, to achieve high ORR catalytic activity, a catalyst should facilitate the formation of O_{ads}; however, in order to facilitate product desorption, the catalyst should not bind these species too strongly. Recently, both theoretical calculations and experimental results have shown that oxygen binds more strongly to Pd than Pt.[20] Due to the high adsorption strength of O_2 on Pd, the O-O bonds can be broken easily, but this generates high O_{ads} coverage.[21] A decrease in the electron density of Pd, which may weaken the Pd-O bond, could substantially enhance the dissociative adsorption of O_2.[22] The strong coupling between the Pd NPs and rPOM support in the Pd/rPOM hybrid results in the transfer of electrons from the Pd NPs to the rPOM, weakening the Pd-O bond. As shown in Fig.

7, the incorporation of rPOM did markedly alter the electronic structure of Pd. For instance, the electron binding energy for the Pd 3d peak of Pd/rPOM (Fig. 7a, black curve) is shifted positively ~0.48 eV relative to the energy observed for the Pd/C material (Fig. 7b, black curve). Considering the similar particle size and morphology of the Pd NPs in the Pd/rPOM and Pd/C catalysts, this shift in binding energy is most likely caused by electron delocalization between the Pd d-orbitals and the rPOM support, as well as by partial ionization due to electron transfer from Pd to rPOM.[23] The electron delocalization between the Pd NPs and rPOM changes the electronic structure of the Pd NPs, decreasing the electron density (down-shift of the d-band centre) of Pd, weakening the Pd-O bond and making the Pd surface easily accessible for O_2 adsorption and activation. On the other hand, the binding energy of the Mo 3d electrons in Pd/rPOM was negatively shifted in comparison to POM (as shown in Fig. 2), which further indicates the strong interaction between Pd and rPOM in the Pd/rPOM hybrid nanomaterials.

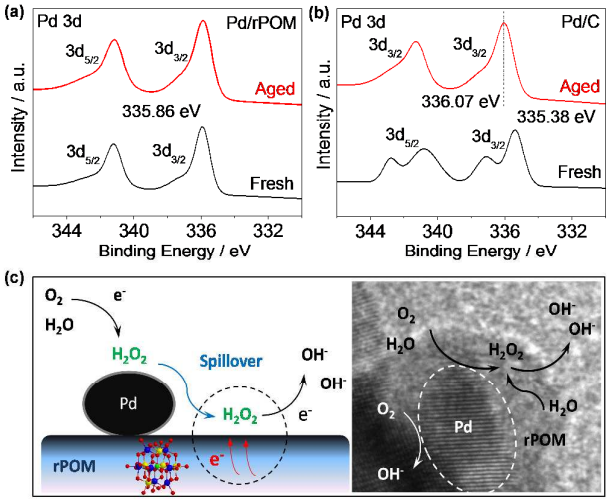

Fig. 7 Pd 3d XPS spectra of (a) Pd/rPOM before and after the durability cycling and (b) Pd/C before and after the durability cycling; (c) Schematic illustration of ORR on interface of Pd/rPOM hybrid with synergistic catalysis.

In addition, the rPOM component of the Pd-rPOM hybrid, aside from being a robust support material for Pd NPs, can also serves as an assistant catalyst for Pd, with a mode of action based on the "dual site functionality ORR mechanism", in which rPOM induces reductive decomposition of undesirable O_{ads}. A schematic illustration of the ORR on the Pd/rPOM catalyst is given in Fig. 7c. The Pd supports the initial adsorption of the O_2 molecule and conversion of O_2 to O_{ads}. The O_{ads} that are formed on Pd sites can be spilled-over to the rPOM sites, where they are further reduced to produce OH^-. The function of the rPOM support as a H_2O_2 decomposition catalyst was confirmed by RDE measurements. Fig. S7 shows a comparison of the rPOM, Pd/C, Pt/C and Pd/rPOM electrodes in terms of their catalytic activity toward H_2O_2 reduction. The current increase in the 0.1 M H_2O_2 + 0.1 M KOH electrolyte relative to that in the 0.1 M KOH electrolyte implies that rPOM is catalytically active in H_2O_2 decomposition (Fig. S7a). The onset reduction potential for the Pd/rPOM electrode is higher than for the Pd/C and Pt/C electrodes. Additionally, a higher reduction current density was achieved on the Pd/rPOM electrode (see Fig. S7b). These results indicate that coupling Pd with rPOM effectively improves its catalytic activity toward H_2O_2 reduction. The H_2O_2 decomposition to OH^- is not only critically important for increasing ORR efficiency but also beneficial in terms of the prevention of support material corrosion. Furthermore, the proton-conductive rPOM has a high ionic conductivity that provides a fast release rate of OH^-. The rPOM functions as a mediator facilitating electron transfer to the dispersed Pd sites as well as to the adsorbed oxygen molecules. All these factors combine to significantly boost the catalytic performance of the Pd/rPOM catalyst for the ORR.

Conclusions

In summary, we have developed an efficient strategy for the synthesis of a novel Pd hybrid catalyst demonstrating very high activity for the ORR compared to Pt/C and Pd/C catalysts in alkaline media. The *in-situ*-developed rPOM support offers stable anchoring sites for the formation and subsequent attachment of Pd NPs, enabling the full utilization of the catalyst surface by minimizing the agglomeration of Pd NPs. The experimental results demonstrate that although rPOM alone has very low catalytic activity toward ORR, its Pd hybrid exhibits substantially enhanced catalytic activity. Furthermore, the new catalyst displays better stability than Pd/C and Pt/C, with almost no degradation in catalytic activity observed during the stability test. Further investigations suggest that the catalytic performance enhancement is a result of the changes in the electronic structure Pd induced by synergistic interaction with the rPOM support, which weakens the interaction between Pd and nonreactive oxygenated species, providing more active sites for O_2 adsorption and activation. In addition, the Pd/rPOM hybrid catalyst also shows improved catalytic activity in acidic media (Fig. S7c, d). Synthetic protocols based on this work provide unique opportunities for material design and may provide a viable route to practical and cost effective electrocatalysts for next-generation fuel cells.

Acknowledgements

This work was financially supported by China National 973 program (2012CB215500 and 2012CB720300), and by NSFC of China (Grant Nos. 21436003, 21176271 and 21276291).

Notes and references

1 M. K. Debe, *Nature*, 2012, **7**, 43-51.
2 (a) V. Mazumder, Y. Lee, S. Sun, *Adv. Funct. Mater.*, 2010, **20**, 1224-1231; (b) W. Li, X. Zhao, A. Manthiram, *J. Mater. Chem. A*, 2014, **2**, 3468-3476; (c) L. Xiao, L. Zhuang, Y. Liu, J. Lu, H. D. Abruna, *J. Am. Chem. Soc.*, 2009, **131**, 602-608.
3 (a) N. Arjona, M. Guerra-Balcázar, L. Ortiz-Frade, G. Osorio-Monreal, L. Álvarez-Contreras, J. Ledesma-García, L. G. Arriaga, *J. Mater. Chem. A*, 2013, **1**, 15524-15529; (b) M. Shao, T. Yu, J. H. Odell, M. Jin, Y. Xia, *Chem. Commun.*, 2011, **47**, 6566-6568.
4 (a) W. Ding, M. R. Xia, Z. D. Wei, S. G. Chen, J. S. Hu, L. J. Wan, X. Q. Qi, X. H. Hu, L. Li, *Chem. Commun.*, 2014, **50**, 6660-6663; (b) D. A. Slanac, W. G. Hardin, K. P. Johnston, K. J. Stevenson, *J. Am. Chem. Soc.*, 2012, **134**, 9812-9819; (c) V. Mazumder, M. Chi, K. L. More, S. Sun, *Angew. Chem. Int. Ed.*, 2010, **49**, 9368-9372; (d) N. Abbasi, P. Shahbazi, A. Kiani, *J. Mater. Chem. A*, 2013, **1**, 9966-9972.
5 V. Mazumder, S. Sun, *J. Am. Chem. Soc.*, 2009, **131**, 4588-4589.
6 A. L. Wang, H. Xu, J. X. Jiang, L. X. Ding, Y. X. Tong, G. R. Li, *J. Am. Chem. Soc.*, 2013, *135*, 10703-10709.

7 (a) Z. Li, S. Ji, B. G. Pollet, P. K. Shen, *Chem. Commun.*, 2014, **50**, 566-568; (b) X. Xie, Y. Xue, L. Li, S. Chen, Y. Nie, W. Ding, Z. Wei, *Nanoscale*, 2014, **6**, 11035-11040; (c) H.-Q. Dong, Y.-Y. Chen, M. Han, S.-L. Li, J. Zhang, J.-S. Li, Y.-Q. Lan, Z.-H. Dai, J.-C. Bao, *J. Mater. Chem. A*, 2014, **2**, 1272-1276; (d) Q. M. Kainz, R. Linhardt, R. N. Grass, G. Vilé, J. Pérez-Ramírez, W. J. Stark, O. Reiser, *Adv. Funct. Mater.*, 2014, **24**, 2020-2027.

8 (a) Y. Liu, W. E. Mustain, *J. Am. Chem. Soc.*, 2013, **135**, 530-533; (b) Y. J. Wang, D. P. Wilkinson, J. Zhang, *Chem. Rev.*, 2011, **111**, 7625-7651; (c) A. Kumar, V. Ramani, *ACS Catal.*, 2014, **4**, 1516-1525.

9 (a) L. Guo, S. Chen, Z. Wei, *Journal of Power Sources*, 2014, **255**, 387-393; (b) S. Lu, D. Wang, S. P. Jiang, Y. Xiang, J. Lu, J. Zeng, *Adv. Mater.*, 2010, **22**, 971-976.

10 (a) D. M. Han, Z. P. Guo, Z. W. Zhao, R. Zeng, Y. Z. Shu, H. K. Liu, *Journal of Power Sources*, 2008, **184**, 361-369; (b) Z. P. Guo, D. M. Han, D. Wexler, R. Zeng, H. K. Liu, *Electrochimica Acta*, 2008, **53**, 6410-6416.

11 (a) M. Ammam, *J. Mater. Chem. A*, 2013, **1**, 6291-6312; (b) M. Chojak, A. Kolary-Zurowska, R. Wlodarczyk, K. Miecznikowski, K. Karnicka, B. Palys, R. Marassi, P. J. Kulesza, *Electrochimica Acta*, 2007, **52**, 5574-5581.

12 (a) D. Wang, S. Lu, S. P. Jiang, *Chem. Commun.*, 2010, **46**, 2058-2060; (b) H. Li, H. Zhang, H. Pang, C. Huang, J. Chen, *J. Solid State Electrochem*., 2010, **14**, 2267-2274.

13 S. Ilhan, C. Kahruman, I. Yusufoglu, *J. Anal. Appl. Pyrolysis*, 2007, **78**, 363-370.

14 M. Sadakane, E. Steckhan, *Chem. Rev.*, 1988, **98**, 219-237.

15 J. Chen, S. Liu, W. Feng, G. Zhang, F. Yang, *Phys. Chem. Chem. Phys.*, 2013, **15**, 5664-5669.

16 Z. Bai, L. Yang, L. Li, J. Lv, K. Wang, J. Zhang, *J. Phys. Chem. C*, 2009, **113**, 10568-10573.

17 Z. Awaludin, M. Suzuki, J. Masud, T. Okajima, T. Ohsaka, *J. Phys. Chem. C*, 2011, **115**, 25557-25567; (b) M. M. Jaksic, G. A. Botton, G. D. Papakonstantinou, F. Nan, J. M. Jaksic, *J. Phys. Chem. C*, 2014, **118**, 8723-8746.

18 Y. Lu, Y. Jiang, X. Gao, X. Wang, W. Chen, *J. Am. Chem. Soc.*, 2014, **136,** 11687-11697.

19 (a) J. Zhang, M. B. Vukmirovic, Y. Xu, M. Mavrikakis, R. R. Adzic, *Angew. Chem. Int. Ed.*, 2005, **44**, 2132-2135; (b) J. K. Nørskov, J. Rossmeisl, A. Logadottir, L. Lingqvist, J. R. Kitchin, T. Bligaard, H. Jónsson, *J. Phys. Chem. B*, 2004, **108**, 17886-17892.

20 M. H. Seo, S. M. Choi, J. K. Seo, S. H. Noh, W. B. Kim, B. Han, *Applied Catalysis B: Environmental*, 2013, **129**, 163-171.

21 V. R. Stamenkovic, B. Fowler, B. S. Mun, G. Wang, P. N. Ross, C. A. Lucas, N. M. Marković, *Science*, 2007, **315**, 493-497.

22 (a) A. Sarkar, A. V. Murugan, A. Manthiram, *J. Mater. Chem.*, 2009, **19**, 159-165; (b) V. Stamenkovic, B. S. Mun, K. J. J. Mayrhofer, P. N. Ross, N. M. Markovic, J. Rossmeisl, J. Greeley, J. K. Kørskov, *Angew. Chem. Int. Ed.*, 2006, **45**, 2897-2901.

23 S. Chen, Z. Wei, X. Qi, L. Dong, Y. G. Guo, L. Wan, Z. Shao, L. Li, *J. Am. Chem. Soc.*, 2012, **134**, 13252-13255.

Table of Contents Graphic

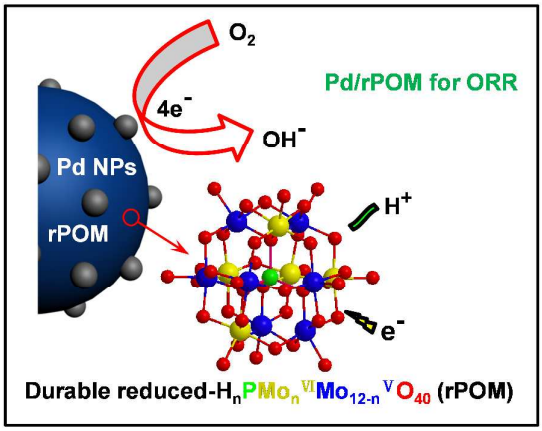

A palladium and reduced-polyoxometalate hybrid catalyst (Pd/rPOM) exhibits excellent electrocatalytic performance for ORR in alkaline media, even better than the Pt/C catalyst.